Review

Direct Solar Thermal Water Splitting Using Iron Electrodes at High Temperatures - A Review

Manuel Fuentes *, Diego Pulido, Edward Fuentealba, Alvaro Soliz, Norman Toro, Atul Sagade, Felipe M. Galleguillos Madrid *

Posted Date: 12 July 2024

doi: 10.20944/preprints202407.1069.v1

Keywords: Solar thermochemical; water splitting; iron corrosion; solar reactors

Review

Direct Solar Thermal Water Splitting Using Iron Electrodes at High Temperatures. A Review

Manuel Fuentes [1,2,*], Diego Pulido [1], Edward Fuentealba [1], Alvaro Soliz [3], Norman Toro [4], Atul Sagade [2] and Felipe M. Galleguillos Madrid [1,*]

[1] Centro de Desarrollo Energético Antofagasta, Universidad de Antofagasta, 1240000, Antofagasta, Chile; diego.pulido@uantof.cl, edward.fuentealba@uantof.cl, felipe.galleguillos@uantof.cl
[2] Departamento de Ingeniería Mecánica, Universidad de Tarapacá, 1100000 Arica, Chile; msfuentes@academicos.uta.cl; asagade@academios.uta.cl
[3] Departamento de Ingeniería en Metalurgia, Universidad de Atacama, Copiapó 1531772, Chile; alvaro.soliz@uda.cl
[4] Facultad de Ingeniería y Arquitectura, Universidad Arturo Prat, Iquique 1100000, Chile; notoro@unap.cl
* Correspondence: felipe.galleguillos.madrid@uantof.cl (F. M. Galleguillos Madrid); Tel.: +56-9-4235-2163 and msfuentes@academicos.uta.cl ; Tel.: +56 9 4526 5145 (Manuel Fuentes)

Abstract: Green hydrogen is a fuel that in the coming years will play a very important role in the energy transition process in developed countries, especially those seeking to reach a level of zero emissions, for which reason its demand is expected to increase significantly. This article analyzes the fundamentals to produce hydrogen, with a focus on the oxidation reaction of a thermochemical solar cycle for the dissociation of water vapor. Solar thermochemical cycles have been extensively investigated, but it is still in the development stage by groups of researchers who have focused on finding the right materials and conditions to improve the efficiency of the process, especially at high temperatures. The theoretical foundations are analyzed, compiled from exhaustive scientific investigations related to the oxidation of iron in water vapor, the relationship with the activation energy of the corrosive process, thermodynamic aspects and the kinetic model according to a heterogeneous reaction. In addition, some high temperature oxidation mechanisms, pH effects, reactors and materials (fluidized beds) used are presented. The scientific review indicates that the production of hydrogen through a thermochemical cycle is more efficient than electrochemical processes (electrolysis), if the limitations of the reduction stage of the cycle are overcome.

Keywords: solar thermochemical water splitting; iron corrosion; solar reactors

1. Introduction

The greatest amounts of insolation are generally found at lower latitudes and in arid climates. The Atacama Desert in northern Chile has exceptionally ideal solar radiation conditions, and the potential for producing green hydrogen is widely acknowledged. As a result, this study aims to lay the groundwork for the synthesis of hydrogen using a thermo-chemical solar process while considering an environmentally favourable, inexpensive, and abundant catalyst material in the region, such as iron oxide. The goal of the research is to discover the theoretical foundations of hydrogen production by iron oxidation at high temperatures, considering the thermodynamic, thermochemical, and electrochemical foundations required to comprehend the heterogeneous reaction. The kinetic modeling of the fluidized bed material inside a thermochemical solar reactor requires this understanding.

The unique solar radiation conditions in the Atacama Desert offer significant potential for various solar technologies, including photovoltaic (PV) systems and concentrated solar power (CSP) plants. PV systems harness the sun's energy directly using solar panels, while CSP plants concentrate sunlight to generate heat and subsequently produce electricity. The desert's high levels of solar radiation allow for enhanced energy capture and conversion efficiency, making it an attractive site for solar power installations.

 doi:10.20944/preprints202407.1069.v1

In addition, the region boasts a stable and predictable climate, with little rainfall and a lack of extreme temperature variations. This climatic consistency is crucial for the long-term performance and reliability of solar energy systems. Furthermore, the desert's vast expanses of land provide ample space for large-scale solar installations, facilitating the deployment of cutting-edge solar technologies and enabling the generation of significant amounts of clean energy. The knowledge gained from studying solar resources in this unique environment not only contributes to advancements in solar technology but also serves as a valuable blueprint for harnessing solar power in other regions with similar radiation characteristics.

Although thermochemical solar cycles using ceria have 25% annual efficiency compared to 14% for the electrolysis process (Alakaline eletrolysis) [1,2], they still present a low level of technological preparation to produce low emission hydrogen [3]. Regarding production costs, it is estimated that hydrogen from solar photovoltaic and wind energy is between 4.0 – 9.0 USD/Kg H_2, and could be below 1.5 USD/Kg H_2, with photovoltaic solar electricity costs of 14 USD/MWh for the year 2030[3].

The essential thing about this review is that it provides the fundamental theoretical information to understand the difficulty that arises when using pure iron or iron oxides as a thermocatalyst material in a thermochemical cycle to produce hydrogen. For this reason, it is important to understand the reaction mechanisms of the material in the presence of water steam from thermodynamics, its identification as a non-catalytic surface heterogeneous reaction from electrochemistry and aspects of the oxidation mechanisms at high temperature considering water vapor as alkaline reactant and the effects of pH on the reaction. In addition, some solar reactors that have used fluidized bed materials are presented. This technical information is intended to provide the reader with data to replicate these reactors, especially for researchers who are just beginning the topic of thermolysis using iron. But at the same time, it shows the potential of its application in a high temperature thermolysis process considering only the oxidation stage.

The scarce information related to the oxidation of iron in the presence of water vapor, a product of the reaction with hydroxyl (OH), generates space for future research with iron and other materials such as copper slag that have iron oxides. Furthermore, because the scientific information collected is mainly based on studies of the reaction of iron with oxygen (O_2).

2. Theoretical Background

In specific thermodynamic conditions, the interaction between water vapor ($H_2O(g)$) and Iron metal (Fe) can lead to the production of Hydrogen (H_2) through the oxidation of Fe in a range of 200 to 1000 °C. This oxidation reaction occurs in an environment abundant in $H_2O(g)$ and is expressed as follows [4]:

$$3Fe + 4H_2O \rightarrow Fe_3O_4 + 4H_2 \quad (1)$$

In 1926, Dunn et al. [5] proposed that the oxidation process at high temperatures is controlled only by the diffusion of O_2 through the oxide layer. The presence of $H_2O_{(g)}$ accelerates the oxidation process of the mild Fe and two grades of pure iron [6].

The H_2 production from the use of Magnetite (Fe_3O_4) was proposed by Nakamura et al. in 1977 [7,8]. However, the production of H_2 by oxidation with $H_2O_{(g)}$ used the concentrated solar radiation was proposed by Lede et al. [9] in 1983. Recent studies have presented notable innovations in the application of solar thermochemical reactors for converting concentrated solar energy into chemical fuels. These advancements involve a two-step thermochemical process specifically designed to produce H_2 from $H_2O_{(g)}$. By harnessing the immense potential of solar energy, this innovative approach offers a sustainable and highly efficient method for generating H_2 fuel. [8,10]. The exothermic reaction from $H_2O_{(g)}$ to produce H_2 is expressed as follows [7,8].

$$3FeO + H_2O \rightarrow Fe_3O_4 + H_2 \quad (2)$$

The Fe_3O_4 produced in this reaction is transformed in a solar oven to FeO through an endothermic sub-process [8,10]. However, a significant barrier arises in this sub-process as a result of the premature fusion of FeO occurring at a lower temperature than the required threshold for the complete thermodynamic cycle. This inherent challenge presents difficulties in effectively employing

 doi:10.20944/preprints202407.1069.v1

a thermochemical solar reactor for the production of H_2, limiting its efficiency and feasibility. The reaction is expressed as follows [7,11].

$$Fe_3O_4(l) \rightarrow 3FeO\ (l) + \frac{1}{2}O_2\ \ ;\ a\ \ T > 1875\ K \qquad (3)$$

High-temperature corrosion is influenced by (i) temperature, (ii) gas composition, (iii) exposure time, and (iv) system pressure, and can be characterized through the thickness reduction (penetration) and the thickness growth rate. The oxidation rate increases significantly during increasing temperature [12], providing a homogeneous medium and improving the thermodynamic equilibrium [13]. The Gibbs free energy is expressed as follows.

$$\Delta G^o = -RT \ln (K) \qquad (4)$$

When a metal is exposed to corrosion at high temperatures in the presence of water vapor, it yields a value of ΔG^o, as determined by equation 5, based on the reaction $xM + yH_2O \rightarrow M_xO_y + yH_2$ [12]. The expression for the Gibbs free energy is as follows:

$$\Delta G^o = -yRT \ln\left(\frac{P_{H_2}}{P_{H_2O}}\right) \qquad (5)$$

Meredig & Wolverton et al. [14] indicate that during the corrosion process, the contact of a metal (M) in contact with steam can produce H_2 by the following expression [14].

$$MO_{(x-1)} + H_2O \rightarrow MO_x + H_2 \qquad (6)$$

Where the expression for the Gibbs free energy is as follows

$$\Delta G^o = \Delta H^{MO_x} - \Delta H^{MO_{(x-1)}} - \Delta H^{H_2O} - T(S^{H_2} - S^{H_2O}) \leq 0 \qquad (7)$$

Where MO_x is the oxidized metal and MO_{x-1} is the reduced oxide.

The water-splitting reaction using FeO as electrode is favorable only at temperature under 800 °C, when $\Delta G° < 0$. The theoretical FeO conversion decreases with increasing temperature [15] and Kodama & Gokon et al.[16] indicate that the oxidation of FeO in the presence of water vapor exhibited a spontaneous reaction ($\Delta G<0$) at temperatures below 1000 K.

Young et al. [17] suggest that various metal oxides can form volatile compounds by direct reaction with water vapor and that hydroxides and oxy-hydroxides can be produced by hydration [18]. On the other hand, Belton & Richardson et al. [19] demonstrate the existence of a volatile iron hydroxide at temperatures exceeding 1300°C. Compared to non-volatile metal oxides, volatile metal oxides exhibit a higher oxygen exchange capacity, which directly correlates with their H_2 production capacity [20].

Table 1 shows the thermodynamic parameters (ΔG^o, ΔH^o, ΔS^o, and T) used to determine the activation energy of the reaction of water vapor with iron, the products of the vapor-dissociation into molecules, ions, and iron oxidation products (oxides and hydroxides). Table 2 shows the typical thermodynamic parameters generated during the reactions oxidation/reduction process of metals in the presence of $H_2O_{(g)}$ at high temperatures.

Table 1. Thermodynamic parameters of Water, Oxides, and Hydroxides.

Chemical species	Gibbs free energy ΔG (kJ/mol)	Enthalpy ΔH (kJ/mol)	Entropy S (kJ/mol)	Temp. K (1 atm)	Ref.
H_2O (l)	-237,1	-285,8	70,0	298	[21,22]
	-228,6	-241,8	188,8	298	[21,22]
H_2O (g)	-214,1	-244,7	213,8	600	[22]
	-198,2	-247,1	228,6	900	
	0	0	130,6	298	[21,22]
H_2 (g)	0	0	151,0	600	[22]
	0	0	163,1	900	
OH^- (aqueous ion)	-157,3	-230,0	-10,7	298	[21]
	34,7	38,9	183,7	298	[22]
OH (g)	29,5	38,9	204,4	600	
	24,9	38,4	216,5	900	
Fe	0	0	27,09	298	[21]

 doi:10.20944/preprints202407.1069.v1

Fe^{2+}	-90,0	-91,1	-107,1	298	[21]
Fe^{3+}	-16,7	-49,9	-280,0	298	[21]
$Fe_{.947}$ O	-244,9	-266,3	56,6	298	[21]
	-245,1	-266,3	57,5	298	[22]
	-224,8	-263,7	93,0	600	
	-205,8	-262,7	115,1	900	
FeO	-251,4	-272,0	60,6	298	[21,22]
	-231,7	-269,4	97,3	600	[22]
	-213,1	-268,4	120,2	900	
Fe_2O_3	-774,4	-826,2	87,4	298	[21,22]
	-742,3	-824,2	87,4	298	[22]
	-661,4	-817,6	173,3	600	
	-585,3	-808,4	235,4	900	
Fe_3O_4	-731,4	-811,6	93,0	298	[23]
	-1012,7	-1115,7	146,1	298	[21]
	-1015,2	-1118,4	146,1	298	[22]
	-914,4	-1107,4	272,1	600	
	-821,8	-1088,6	368,3	900	
FeO (OH)	-491,8	-562,6	60,4	298	[21]
$Fe(OH)_2$	-486,9	-568,9	87,9	298	[22]
	-405,7	-564,1	160,4	600	
	-327,6	-558,9	207,7	900	

Table 2. Thermodynamic Parameters of the Reaction of Iron or Oxides in Water Vapor.

Reaction	Gibbs free energy ΔG (kJ/mol)	Enthalpy ΔH(kJ/mol)	Temp. K (pres. atm)	Ref.
$0.75\,Fe + H_2O \rightarrow 0.25Fe_3O_4 + 4H_2$	-14,52	-32,09	600	[24]
$Fe + 2H_2O \rightarrow FeO + H_2$	-199,3	-	1000	[25]
$Fe + 2H_2O \rightarrow Fe(OH)_2(g) + H_2$	38,9 + 5*80T (cal)	-	-	[19]
$2Fe + 3H_2O \rightarrow Fe_2O_3 + 3H_2$	48,9	-	973 - 1123	[26]
$3Fe + 4H_2O \rightarrow Fe_3O_4 + 4H_2$	11,0	-	973 - 1123	[26,27]
$3FeO + H_2O \rightarrow Fe_3O_4 + H_2$	-	-33,6	873	[15,16,28,29]
$Fe_2O_3 + H_2O \rightarrow 2FeO(OH)$	10,39	-47,54	400	[24]
$Fe_3O_4 + 2H_2O \rightarrow Fe(OH)_2 + 2FeO(OH)$	41,02	-79,23	400	[24]
$Fe_3O_4 + 4H_2O \rightarrow Fe(OH)_2 + 2Fe(OH)_3$	228,22	-120,48	600	[24]
$2Fe_3O_4 + H_2O \rightarrow 3Fe_2O_3 + H_2$	40,5	-	-	[30]
$2Fe_3O_4 + 4H_2O \rightarrow 6FeOOH + H_2$	44,4	-	-	[30]

3. Kinetic Model

The mechanisms in which a pure metal or alloy is oxidized at high temperatures require a series of successive steps [18,31]. The steps are:

Step a) Adsorption of a gaseous component,

Step b) Dissociation of the gaseous molecule and transfer of electrons,

Step c) Nucleation and growth of crystals,

Step d) Diffusion and transport of cations, anions, and electrons through the oxide layer.

However, the reaction between a solid (Fe) and a gas ($H_2O_{(g)}$) corresponds to a heterogeneous reaction where the kinetics is totally or partially controlled for the mass transport process. the product species generate by convection and diffusion process and can be gaseous, or insoluble solid [32]. Diffusion and heat transfer are phenomena that intertwine with the chemical kinetics of non-catalytic

 doi:10.20944/preprints202407.1069.v1

heterogeneous reactions, with their respective diffusion equations extending to fluidized solids [33]. The reduction of iron oxide with hydrogen or the oxidation of iron with steam serve as two typical examples of this type of reaction. However, these reactions occur under the conditions of a highly compacted unreacted solid with limited porosity, where the chemical reaction proceeds rapidly while diffusion proceeds relatively slowly [34].

Wen et al. [34] consider that a superficial non-catalytic heterogeneous reaction consists of the following steps (Figure 1):

Step a) diffusion of fluid reactants through the fluid film surrounding the solid.

Step b) diffusion of the fluid reagents through the porous solid layer.

Step c) adsorption of the fluid reagents on the surface of the solid reagent.

Step d) chemical reaction with the solid surface,

Step e) desorption of the fluid products from the solid reaction surface.

Step f) diffusion of the product far from the reaction surface through the porous surface, solid media, and through the fluid film surrounding the solid.

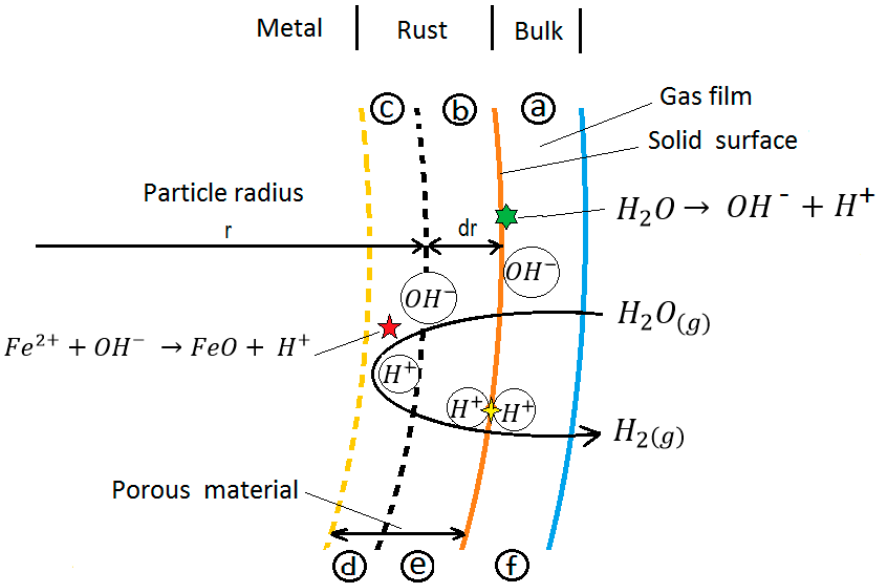

Figure 1. Step diagram of the non-catalytic superficial heterogeneous reaction of the electrochemical dissolution of iron in water vapor.

The study involved to Surman et al. [35] accomplishing the oxidation of pure Fe at 500°C using hydrogen, water vapor or various mixtures of hydrogen-vapor. The oxidation kinetics were compared with models of chemical diffusion and solid-state reactions. The diffusion of volatile iron in the form of $Fe(OH)_2$ played a crucial role as the rate-controlling step. This diffusion occurred from the metal-oxide interface through the porous oxide of the inner layer, ultimately depositing Fe_3O_4 on the crystals of the outer layer, which acted as sinks.

The oxidation kinetics was approximated to the parabolic law, and the vapor phase transport hypothesis led to the expression of the parabolic rate constant (K_w), represented by the following expression.

$$K_w = 4.8 * 10^4 * F_p * T^{1/2} * \left(\frac{P_{H_2O}}{P_{H_2}}\right) * e^{-38900/RT} \quad (8)$$

Where, K_w is the parabolic rate constant in (g^2/m^4s) and F_p is the porosity factor of the inner layer, P_{H2O}, and P_{H2} are the partial pressures of H_2O and H_2 respectively.

Park et al. [36] studied the hydrogen production used iron oxide and inert silica with $H_2O_{(g)}$ under temperatures between 460-700°C and vapor partial pressure between 0.002-0.02 MPa. Whence, the Fe is oxidized to Fe_3O_4 (first step), then Fe_3O_4 is gradually oxidized to Fe_2O_3 in the second step, researchers have if the $H_2O_{(g)}$ is in the equilibrium state of adsorption and that the reaction rate-determining step is the desorption of hydrogen from the active sites.

 doi:10.20944/preprints202407.1069.v1

The proposed initial oxidation rate when the partial pressure of water is fixed and is represented by the following expression.

$$\left(\frac{dX_B}{dt}\right)_{t=0} = \left(\frac{bk}{1+K_{e\_ads}P_{H_2O}}\right)P_{H_2O} - \frac{\left(\frac{bk}{1+K_{e\_ads}P_{H_2O}}\right)}{K_e}P_{H_2} \quad (9)$$

Where, b is the stoichiometric coefficient of the oxidation reaction of Fe to Fe_2O_3, k is the overall rate constant based on unit solid volume, K_e is the chemical equilibrium constant, K_{e_ads} is the equilibrium adsorption constant, P_{H2O}, and P_{H2} are the partial pressures of water and hydrogen respectively.

The heterogeneous kinetic models are explained in detail by Donovan & Berra et al. [37], Levenspiel et al. [38], and Klaewkla et al. [39]. However, Wen & Wang et al. [40] propose a kinetic model of the non-catalytic heterogeneous reaction in a solid-gas reaction system considering the heat and mass transfer as combined effects.

Valipour & Saboohi et al. [41] analyzed multiple mathematical models and developed a comprehensive model for a multi-reactant system utilizing porous granules within a sample of a mobile packed bed. Our model takes into account various factors, including external mass transfer, internal diffusion through the pores, chemical reactions, heat generation or consumption due to reactions, and heat transfer via effective conduction throughout the solid matrix.

The three main types of growth laws that have been established experimentally, linear, parabolic and the logaritmic law are illustrated in Table 3, this equations represent the oxidation reaction rate of a metal at high temperatures published in popular science magazines.

Table 3. Reaction rate equations, applicable to high-temperature oxidation.

Equation	Observation	Ref.
	Logarithmic reaction rate:	
$X = K_{reaction}\ln(t + t_o) + A$	It represents the initial oxidation states at low temperatures.	[31]
$X = K_{reaction}\ln(Bt + 1)$	-	[31]
	Lineal reaction rate:	
$\frac{dx}{dt} = K_{Lineal}$	It represents a constant rate of oxide growth applicable at very high temperatures.	[31]
$X = K_{Lineal}t + C_{Lineal}$	-	[31]
$\Delta W/_A = K_L\, t$	-	[42]
	Parabolic reaction rate:	
$\frac{dX}{dt} = \frac{K_{Parab}}{x}$	It adjusts to the processes controlled by the diffusion of species.	[31]
$X^2 = K_{parab}t + C_{parab}$	-	[31,43]
$\left(\Delta W/_A\right)^2 = K_{parab} * t$	-	[42]
$\frac{dX}{dt} = k\, f(X)$	The function f(X) depends on the reaction mechanism for diffusion in one, two, or three dimensions.	[44]
$\frac{dX}{dt} = k(T) * f(X)$ $k(T) = k_o * e^{\left(\frac{-E_a}{RT}\right)}$	The reaction rate of a sample of iron slag in water vapor.	[45]

Where:

X: the thickness of oxide consumed per surface unit or the weight gain per area unit.

ΔW/A: the mass gain per unit area (g/cm^2)

t: is the time.

k(T): the reaction rate constant.

 doi:10.20944/preprints202407.1069.v1

f(X): function that represents the reaction mechanism.
ko, $K_{reaction}$, K_{Lineal}, K_{Parab}: reaction constants.
E_a: is the activation energy.
R is the gas constant.
T is the absolute temperature.
A, B: constants.
C_{Lineal}, C_{Parab}: constants of integration.

The Fe oxidation kinetic follows a linear-parabolic behavior in the presence of $H_2O_{(g)}$, suggesting a transition process, where the diffusion of the hydroxyl ion is a determining factor in the kinetic during the oxidation process [42]. Fujii & Meussner et al. [46] indicated that the kinetic oxidation of iron at 1100°C can adjusted to a parabolic law during the first 3 hours and later a lienar behavior is established, where increase the weight per unit area of the all specimes (rate of weight gain was 6,2 mg/cm² hr.). The effect of temperature on the reaction rate is obtained by applying the Arrhenius and is represented by the following expression [44,45].

$$K = K_o e^{\frac{-\Delta G^o}{RT}} \quad (10)$$

Where K is the equilibrium constant, K_o is the reaction constant, ΔG^o is the activation energy, R is the gas constant, and T is the absolute temperature, respectively.

If the reaction rate is governed by diffusion in the solid state through the oxide layer. During the diffusion process, the oxide thickness (rust) increase, but at the same time the kinetic decreases with time [31]. In the cathodic subprocess occur the reaction $2H_2O_{(g)} + 2e^- \rightarrow 2OH^- + H_2$ product of the high temperature dissociation process. The scientific literature indicates that the formation of OH^- from $H_2O_{(g)}$ is proportional to the concentration of $H_2O_{(g)}$ and that the appearance of OH^- cannot be interpreted in terms of the simple dissociation of $H_2O_{(g)}$. It is necessary to consider the pathway that involved in the formation of intermediate products generated during ORR such as (i) H_2O_2, and (ii) HO_2^- [47].

4. High-Temperature Oxidation Mechanisms

Despite the extensive scientific information on the oxidation of iron at envioromental temperature and at high temperature due to the presence of the oxygen ion and in order to reduce or avoid iron corrosion, it is still not clear enough what the mechanism of electrochemistry reaction that explains the presence of oxides such as FeO, Fe_3O_4 and Fe_2O_3, especially when iron interacts with the hydroxyl ion (OH^-).

Shrinivasan et al. [48] developed a multi-step optical system that enables water decomposition for OH^- ion detection, demonstrating that rate constants can be accurately measured at lower temperatures such as 500 K. This stands in contrast to alternative methods that necessitated temperatures exceeding 2570 K [49].

Lede et al. [9] propose a kinetic mechanism of thermal dissociation of H_2O between 2000 – 3000K represented by the following expressions.

$$H_2O + G \leftrightarrow H + OH + G \quad (11)$$
$$H_2O + H \leftrightarrow H_2 + OH \quad (12)$$
$$OH + H \leftrightarrow H_2 + O \quad (13)$$
$$OH + O \leftrightarrow O_2 + H \quad (14)$$

Where, G is the extinguishing gas (argon at room temperature or steam at 400 – 450K and between 2.5 - 9.4 bar, H is the H^+ and OH is the OH^- ions, respectively.

Fe corrosion is an electrochemical dissolution process that produces an electron transfer to an intermediate species formed by the interaction between ferrous ions and water. In the reduction of Fe, the intermediate species is found on the iron surface and must continue to react in a second reaction to form Fe [50].

The initial rate of oxidation of a newly exposed surface of Fe or steel recently exposed to $H_2O_{(g)}$ is always lower, if we compare it to the rate of corrosion generated by O_2. Since the trend is for H_2 to dissolve in solid metals in the atomic form, rather than the molecular form, according to researchers

Preprints.org (www.preprints.org) | NOT PEER-REVIEWED | Posted: 12 July 2024 doi:10.20944/preprints202407.1069.v1

Tuck et al. [6,42] it would seem unlikely that H_2 would dissolve in an oxide network, as it is too large to diffuse, so they suggest that the cathodic reaction could occur within the scales.

Equation 15 shows the general reaction for the production of H_2 gas.

$$2H_2O + 2e^- \rightarrow 2OH^- + H_2 \quad (15)$$

The mechanism of evolution of H_2 (HER) would occur on the surface of the pores and micropores where the hydroxyls (OH^-) formed by the dissolution of the vapor are discharged through a cathodic reaction according to Figure 2.

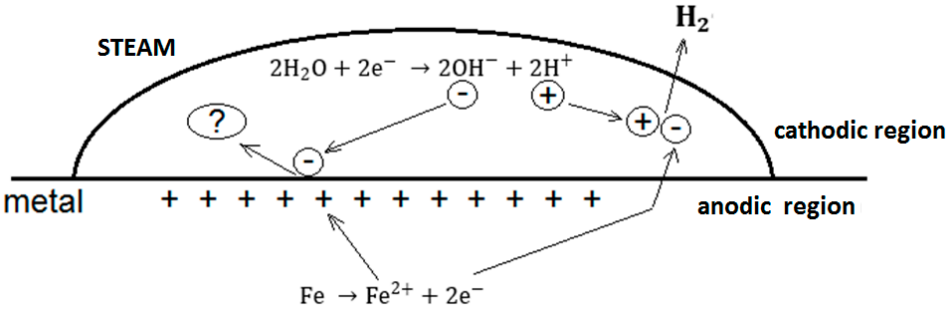

Figure 2. Diagram of the electrochemical dissolution of iron.

Rahmel & Tobolski et al. [51] proposed that the oxide layer is still thin and malleable in the first step the of oxidation process. In the presence of $H_2O_{(g)}$, the transport mechanisms are specifically through cavity or pore formation is probably to occur. The mechanism is represented by Figure 3.

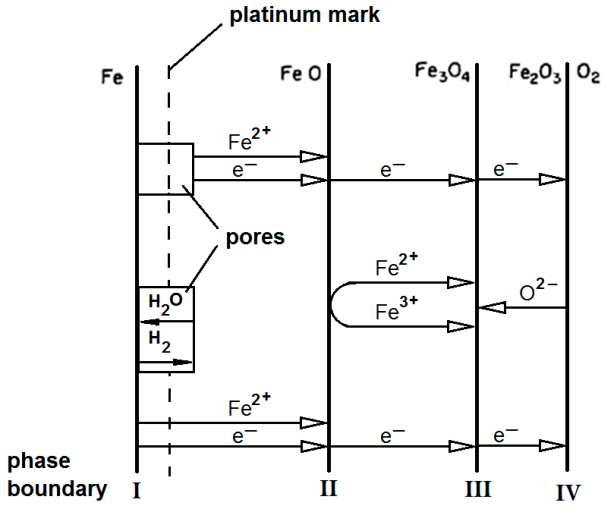

Figure 3. The mechanism in O_2-H_20 vapor mixtures after long periods (adapted from [51].)

Schuetze et al. [27] proposes that the $H_2O_{(g)}$ is involved in the transport processes that lead to scale growth in the oxide layer. The researchers indicate, the Fe cations (Fe^{2+}/Fe^{3+}) can simultaneously diffuse towards the outer surface in this process.

In particular, in the large pores in the inner part of the scale of FeO, a circulation mechanism is assumed that consists of the oxidation of Fe in contact with $H_2O_{(g)}$, thus releasing H_2 that can move back in the pore towards the outer part of the scale, where it reduces the oxide thus forming a $H_2O_{(g)}$ molecule again (Figure 3 and Table 4).

Preprints.org (www.preprints.org) | NOT PEER-REVIEWED | Posted: 12 July 2024 doi:10.20944/preprints202407.1069.v1

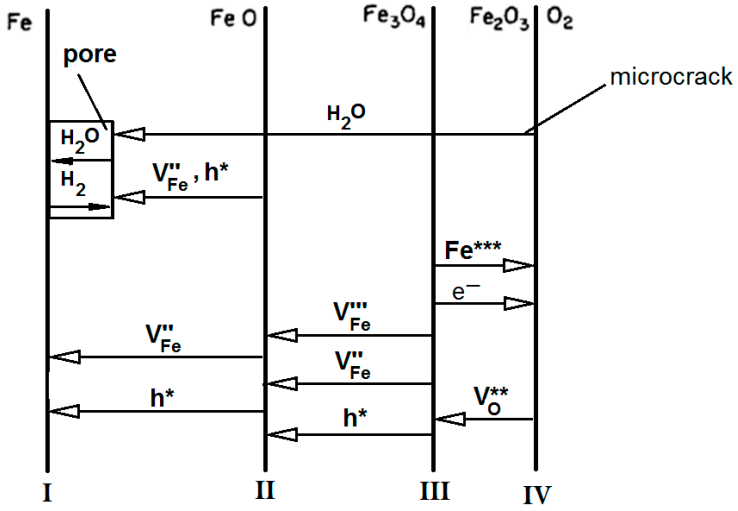

Figure 4. Schematic diagram of the transport processes in the growth of oxide scales on iron for oxygen atmospheres containing H_2O (adapted from [27]).

Table 4. The nomenclature used in the transportation process was proposed by Schuetze [27].

Nomenclature	Meaning
V'''_{Fe}	Fe^{3+} vacancy on a catión position
V''_{Fe}	Fe^{2+} vacancy on a catión position
h^*	h^+ electron-hole
V^{**}_{O}	O vacancy on an anion position
Fe^{***}	Fe^{3+} ion on an interstital position

Based on the knowledge of the structure and diffusion of iron oxides, the oxidation mechanism of pure iron above 570 °C in an iron-oxygen systems are shown in Figure 5 [52], Figure 6, and Table 5 [42].

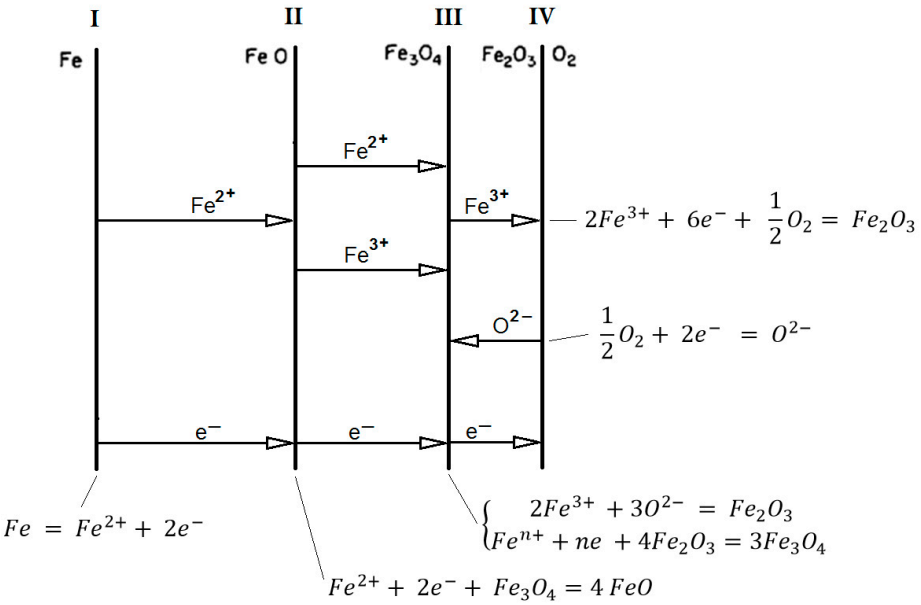

Figure 5. Iron oxidation mechanism showing diffusion of various ionic species (adapted from [52,53]).

Preprints.org (www.preprints.org) | NOT PEER-REVIEWED | Posted: 12 July 2024 doi:10.20944/preprints202407.1069.v1

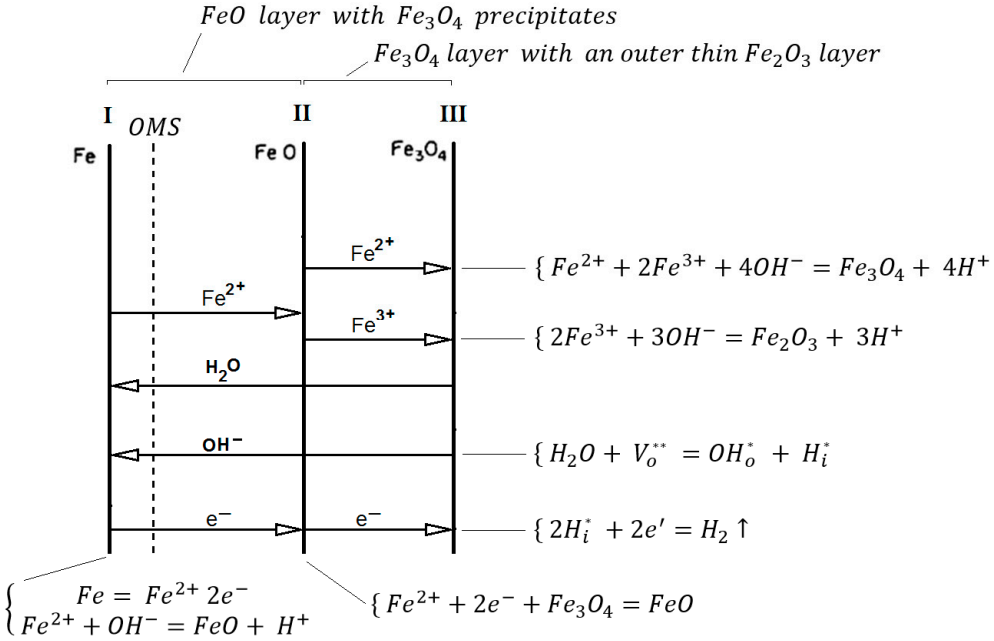

Figure 6. Mechanism of Fe oxidation processes in steam (adapted from [42].)

Table 5. Transport process nomenclature proposed by Yuan et al. [42].

Nomenclature	Meaning
V_O^{**}	Fully ionized oxygen vacancy
OH_O^*	Substitutional hydroxide ion
H_i^*	h^+ electron-hole
e'	Electron
OMS	Original Metal Surface

The first reaction that occurs is from the formation of OH^- ions, which would increase cation vacancies (eq.16) and would also be the main diffusion species [5,6,42].

$$Fe + 2H_2O \rightarrow Fe^{2+} + 2OH^- + H_2 \quad (16)$$

Yuan et al. [42] suggest the formation of ferrous oxide (FeO) (eq.17, Figures 7 and 8), that is, iron in the presence of water vapor at high temperatures will precipitate FeO and Fe_3O_4 [42] or Fe_2O_3 [26].

$$Fe^{2+} + OH^- \rightarrow FeO + H^+ \quad (17)$$

However, FeO in contact with $Fe(OH)_2$ [54] is generated at temperatures above 1300°C [19] and can form Fe_2O_3 in conjunction with the release of H_2 gas [42].

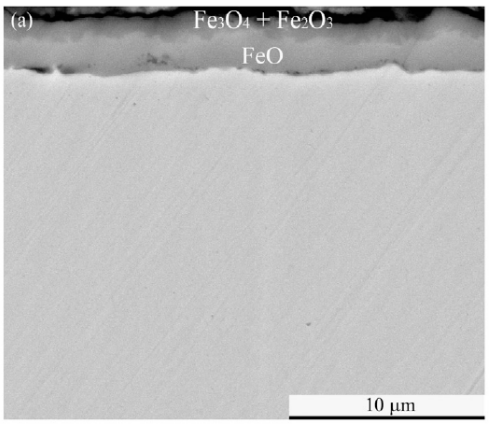

Figure 7. Cross-sectional SEM image of oxides formed on iron after 1 h of oxidation at 650 °C [42].

 doi:10.20944/preprints202407.1069.v1

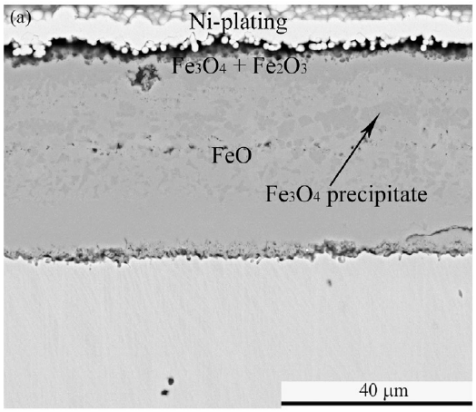

Figure 8. Cross-sectional SEM image of oxide scale formed on iron after 10 h of steam oxidation at 650 °C, where the outermost white layer is nickel-plated [42].

Rahmel & Tobolski et al. in 1965 [51] proposed the existence of pores at the Fe/FeO interface during the oxidation process, forming oxide bridges from the metal to the scale, which allows further oxidation of the metal without substantial inhibition. A mixture of H_2/H_2O is formed in these pores and through an oxidation/reduction mechanism O_2 is transported to the Fe surface.

An oxide of the Fe_nO_m type will normally contain a variety of defects. These defects are responsible for the transport of material through the oxide layer and therefore play a critical role in the oxidation process [6,55].

Yuan et al. [42] indicate in their research that during the initial period (before 5 hours), the existence of a single layer of columnar grains may allow relatively fast transport of OH- ions across grain boundaries. Therefore, it is valid to assume that the hydroxyl ions interact with the surface Hematite and Magnetite, forming FeO.

However, some aspects remain to be investigated, such as that proposed by Stehle et al. [56], who indicate that at typical reaction temperatures (T> 327 °C), the mobility of oxygen and metal ions is expected to be very high, so diffusion limitations are not considered significant, except for the oxides that exceed the thickness of several microns, where the potential of iron III must be considered (eq.18) [42,56,57].

$$4O^{2-} + 2Fe^{3+} + Fe^{2+} \rightarrow Fe_3O_4 \quad (18)$$

Another aspect that should be considered is what was stated by Saunders et al. [18], who indicate that the oxide growth, including the adsorption, dissociation, and diffusion of the reagents, are altered in the presence of water vapor, for which reason it will imply considering thermodynamics, the development of microstructures and the processes of transport. Table 6 shows the standard reduction potentials that have been considered in the electrochemical analyzes of the oxidation of iron and iron oxides in steam.

Table 6. Standard Reduction Potential.

Half reaction	Standard Reduction Potential, E° (V)	Ref.
$H_2 \rightarrow 2H^+ + 2e^-$	E° = 0,000 (V)	[58]
$Fe \rightarrow Fe^{2+} + 2e^-$	E° = - 0,447 (V)	[58]
Reaction		
$3Fe + 4H_2O \rightarrow Fe_3O_4 + 4H_2$	-	[45]
$2FeO + H_2O \rightarrow Fe_2O_3 + H_2$	E° = 0,356 (V)	[45]
$2Fe_3O_4 + H_2O \rightarrow 3Fe_2O_3 + H_2$	E° = 0,210 (V)	[30]
$2Fe_3O_4 + 4H_2O \rightarrow 6FeOOH + H_2$	E° = 0,230 (V)	[30]

 doi:10.20944/preprints202407.1069.v1

From these reactions, electrochemical reaction kinetics can be understood due to the importance it has for the application of metal oxide redox reactions in energy conversion systems such as chemical loop systems and H_2 storage [59].

In an activation regime, the speed of the electrochemical process is due to the transfer of electrons as the only variable that controls the speed of the global process [31], so the corrosion reaction can be expressed by the ionization of a metal. But the possibility that this reaction occurs spontaneously under real conditions forces us to study the energy changes associated with the reaction.

However, some H^+ ions migrate into the metal-forming H_2, therefore, the presence of H^+ ions can promote stress corrosion cracking, through the process of hydrogen embrittlement [60].

FeO nucleation and growth are enhanced by increasing oxygen pressure [55,61]. Kogan et al. [62] studied the dissociation of water at temperatures of 2000, 2200, 2500, and 2800 K, and a pressure of 0.05 (bar), and determined that 25% (at 2500K) and 55% (at 2800 K) of the Water vapor dissociates at constant pressure, increasing at high temperatures.

Kodama et al. [63] indicates that the separation of water by a thermochemical process at a pressure of 0.01 bar and 2000K is barely perceptible, and by increasing the temperature to 2500K, the yield of H_2 exceeds 15% at the same pressure. Young et al. [17] proposed that in pure steam or mixtures of water vapor and inert gas, the equilibrium value of p_{O2} (oxygen pressure) is determined by the degree of dissociation of H_2O, and that, in the case of pure steam, the dissociation of one mole of water produces x moles of H_2 and x/2 moles of O_2, and x is calculated from the equilibrium expression shown in Equation 19.

$$K_1^2 = \frac{x^3}{2(1-x)^2\left(1+\frac{x}{2}\right)} P_T \quad (19)$$

Where P_T is the total pressure and since K_1 is small (x << 1), therefore the before expression approaches:

$$x = \left(\frac{2K_1^2}{P_T}\right)^{1/3} \quad (20)$$

$$p_{O_2} = xP_T \quad (21)$$

Ehlers et al. [64] propose that $Fe(OH)_2$ formed within oxide scales at low oxygen pressure (P_{O2}), migrates to the outer surface, where due to higher pressure hematite (Fe_2O_3) is formed. Khanna et al. [52] propose that iron in the presence of oxygen when oxidized forms a mixed scale of three oxides (FeO, Fe_2O_3, Fe_3O_4), whose composition varies with the temperature and with the partial pressure of O_2 according to the iron phase diagram (Figure 9).

Ketteler et al. [65] in their research, consider a Fe-H_2O system, to determine the stability of iron oxide as a function of the partial pressure of water, indicating as the phase limit for water condensation the range 125 K ($1x10^{-11}$ mbar) up to 373K (1 bar). The calculated phase diagram is presented in Figure 10, as a function of oxygen pressure and temperature, according to the equilibrium constant of dissociation of water ($2H_2O \rightarrow 2H_2 + O_2$), according to equation 22. The researchers conclude that water in its gaseous state acts as an oxidizing compound and that the stability of iron oxides is determined by the partial pressure of the decomposition of water into hydrogen and oxygen.

$$k_1 = \frac{p_{O_2} p_{H_2}^2}{p_{H_2O}^2} \quad (22)$$

Preprints.org (www.preprints.org) | NOT PEER-REVIEWED | Posted: 12 July 2024 doi:10.20944/preprints202407.1069.v1

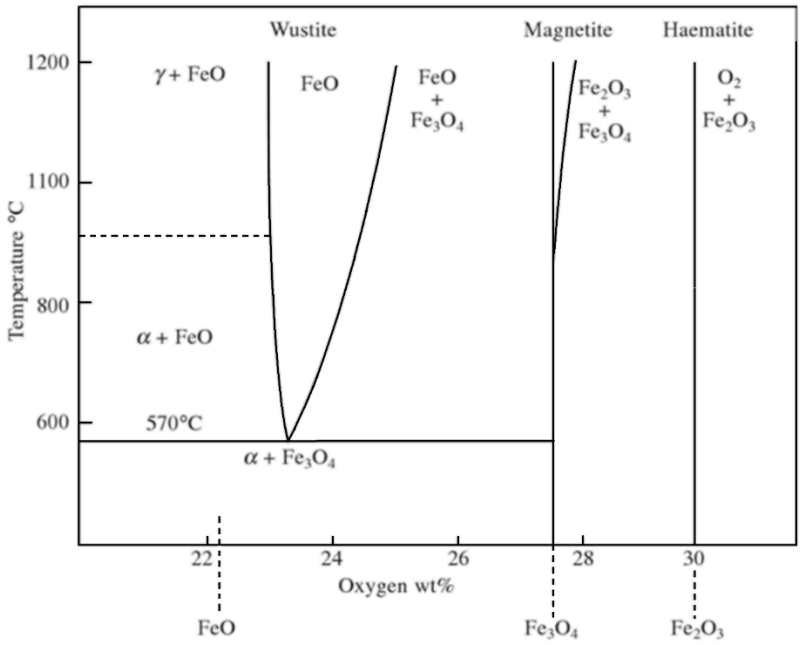

Figure 9. Phase diagram, depicting the stability of various iron oxides as a function of oxygen pressure and temperature [52,53].

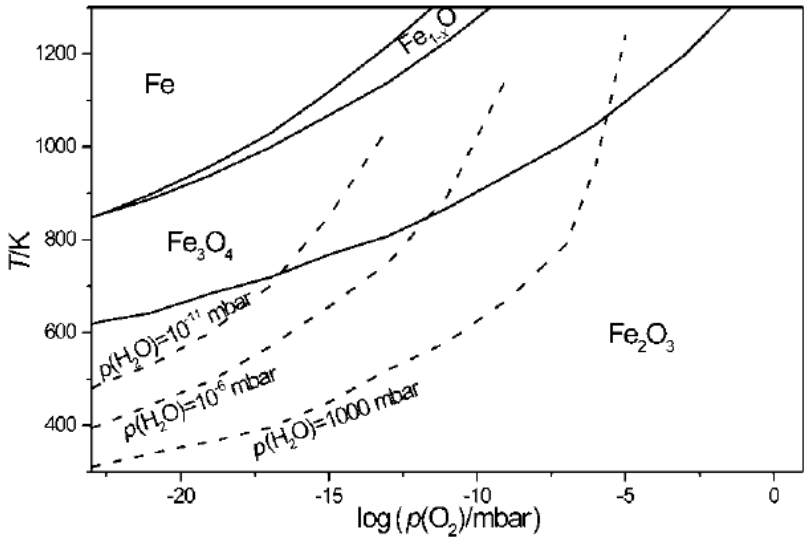

Figure 10. The phase diagram in a water atmosphere represents the stability of iron oxides [65].

5. Effect of pH on Oxidation and Temperature

The pH value is normally based on the equilibrium reaction of the dissociation of water ($H_2O \rightarrow H^+ + OH^-$), this reaction has an endothermic character, and its equilibrium shifts to the right side with increasing temperature.

Research indicates that at the temperature of 300°C (25 MPa), the concentrations of both H^+ (stable in acidic solutions) and OH^- (stable in basic solutions) [60] are approximately three orders of magnitude above those values of water at ambient temperature. Therefore, water has been considered both acidic and alkaline [66].

To produce green hydrogen from a thermochemical process (thermolysis), it is necessary to reach temperatures in the range of 800 – 1400 °C in the reactor [67], this temperature range has been reached in a solar thermal concentrator system of down beam.

Preprints.org (www.preprints.org) | NOT PEER-REVIEWED | Posted: 12 July 2024 doi:10.20944/preprints202407.1069.v1

Iron as a material for obtaining hydrogen has been considered for the thermochemical solar process because the conversion of Fe_3O_4 to FeO improves significantly with higher thermal reduction temperatures [42]. However, its application is complicated because in a thermochemical cycle (thermal reduction stage) the fusion of Fe_3O_4 occurs at temperatures above 2227°C (Figure 11) [7,68] and FeO melts at temperatures as low as 1370 [11] or 1400°C [16]. These factors complicate the design and operation of thermochemical reactors (STWS) based on Fe_3O_4/FeO [11]. But the thermal oxidation stage (hydrolysis) is carried out at temperatures between 200 – 1000°C [4,7,10,28,56]. According to the scientific literature, the temperature affects the process because the oxidation of iron by steam is thermodynamically favorable in the range of 127-527 °C [11,24] or in the temperature ranges of 650-750 °C. [42], 700-850 °C [26], but reaction temperatures in the range of 717 to 1127 °C [57] have also been investigated.

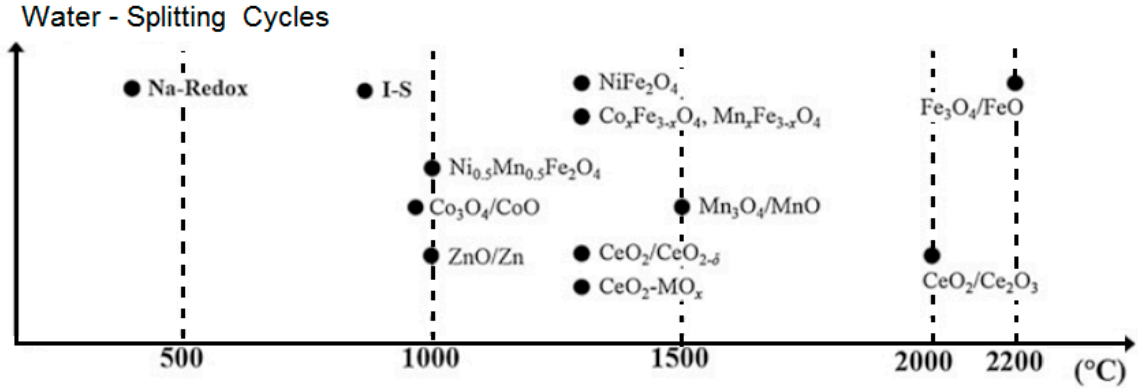

Figure 11. Operating temperature of typical thermochemical water splitting cycles in the reduction stage (adapted from Hiroki Miyaoka, 2016) [68].

6. Material Used in Fluidized Bed

It is important to highlight that the selection of iron oxide is because it is an environmentally friendly base material, with a relatively low cost and that it is generally used in the redox reaction due to its high oxygen-by-weight ratio in mass with sufficient reaction time [44].

From the reviewed scientific literature, it was determined that a temperature above 1300°C can be obtained when using a thermochemical solar reactor and some metallic material (cerium oxide or zinc oxide) in a fluidized bed [67,69]. The thermal powers obtained in reactors that use water-steam and different types of material in a fluidized bed are presented in Table 7. The iron oxide materials investigated for the separation of water in the oxidation stage at the laboratory level are presented in Table 8.

Gokon et al. [29], observed that the hydrogen production rate after steam injection reached a maximum value of 12.3 Ncm^3/min at 25 min, after which the hydrogen production rate decreased rapidly. This shows that the production of hydrogen through a fluidized bed is feasible.

Below is presented in Table 9, a list of thermochemical solar reactors, which have used a fluidized bed material and different gases for fluidization, considering the geometry of the reactor and the material used for its construction.

Table 7. Temperatures reached in a Thermochemical Solar Reactor with Fluidized Bed.

Thermal Power	Temperatures reached or required	Thermal Fluid	Fluidized Bed Material	Particle Size (μm)	Ref.
1 kW_{th}	1300 °C	Water/Steam	Coal – coke	140 (200-300) (300-500) (500-710)	[63,70–72]

 doi:10.20944/preprints202407.1069.v1

10 a 20 kW_{th}	2200 °C	Water/Steam	ZnO reagent powder	1 - 5	[73]
3 MW_{th}	1500°C.	Water/Steam	Cerium Oxide Material	< 300 (100 – 300)	[28,67,74,75]
110 kW_{th}	1400 °C	Gases	Non-stoichiometric cerium oxide particles	10 - 210	[69,76]
100 kW_{th}	960 – 1100 °C	Air	Quartz sand particles	100 - 500	[77]
250 kW_{th}	800 – 1000°C	Air	A mixture of coal-coke and quartz sand	100-300 (coal) 100 – 700 (sand)	[78]
30 kW_{th}	560 °C.	Air	A mixture of sand and basalt		[79]
450 kW_{th}	770 °C.	Air	Isotropic materials		[80,81]
140,63 W_{th} (2kW_e) 231,32 W_{th} (4 kW_e)	250 °C	Air	Sand, ceramic casting media (carbo Accucast ID50) y SiC		[82]

Table 8. Iron Oxide Materials.

Iron Oxides Material		Sample/Particle Size (μm)	Temp. (°C) (time)	Partial Vapor Pressure	Thermal Fluid (flow)	Ref.
Magnetite	Fe_3O_4	30 -50 100 -125	575 673	-	-	[16,63]
The partial substitution of iron in Fe_3O_4 by Ni, Co, and Zr, to form mixed metal oxides.	$(Fe_{(1-x)}M_x)_3O_4$ $NiFe_2O_4$ $NiFe_2O_4$/m-ZrO_2	Sample in a quartz tube	1000	-	-	[16,28,63]
Magnetite supported on zirconium stabilized with cubic yttria	Fe_3O_4/c-YSZ	Ceramic foam	1100 (80 min)	75% of the steam pressure at 90°C, 1 bar	H_2O/N_2 (10 Ncm^3/min)	[76]
Commercial nickel ferrite supported on zirconium oxide	$NiFe_2O_4$/ ZrO_2	Sample on Pt cup	1000 (60 min)	steam pressure at 80°C, 1 bar	H_2O/N_2 (4 mL/min)	[83]
Unsupported Commercial Nickel Ferrite	$NiFe_2O_4$	212 -710	1,6 – 1,7 kW_{th} (10 - 92 min)	51%(0,51 atm) of the steam pressure at	H_2O/N_2 (0,24 Ndm^3/min)	[29]

 doi:10.20944/preprints202407.1069.v1

				82°C, 1 atm		
Monoclinic magnetite supported on zirconium substrates	Fe_3O_4/m-ZrO_2	Polished Fe Bar without oxidation	397 – 602 (180 min)	-	Nitrogen (100 cc/min) Argon (200cc/min) Liquid water (12,5 µL/min)	[56]
iron oxide with various support materials, ZrO_2, CeO_2, yttria-stabilized zirconia (YSZ), and gadolinia-doped ceria (GDC)	Fe_2O_3/ZrO_2 Fe_2O_3/CeO_2 Fe_2O_3/YSZ Fe_2O_4/GDC	150 -300	550	-	H_2O/Ar (prop. 5:95) (300 mL/min)	[59]

Table 9. Technologies of thermochemical solar reactors with fluidized bed.

Reactor Geometry	Bed /gas	Material	Reactor	Year/ Ref.
Diameter=5cm Height= 32cm	Charcoal /CO_2	Silice glass tube	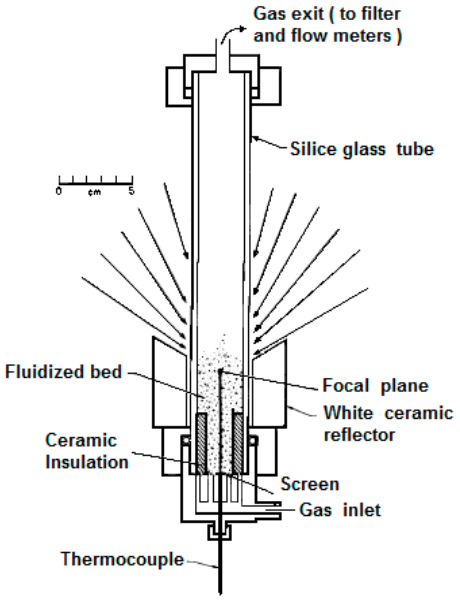	1983 [84]
	ZrO_2, SiC /aire,N_2,CO_2	clear quartz tube	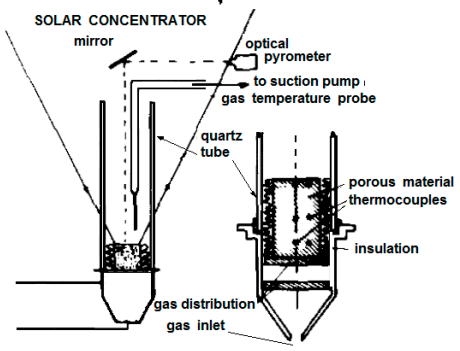	1983 [85]

Preprints.org (www.preprints.org) | NOT PEER-REVIEWED | Posted: 12 July 2024 doi:10.20944/preprints202407.1069.v1

0.90 m high, 0.78 m wide, with a radius of curvature of 0.78 m	alumina particles/air	refractory stainless steel (AISI 310)	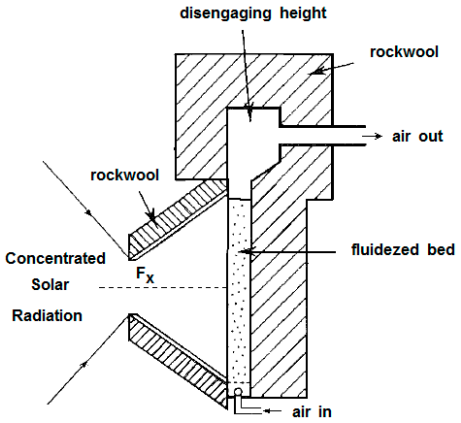	1988 [86]
Diameter= 2cm	$ZnO+Al_2O_3$/ CH_4+Ar	quartz tube	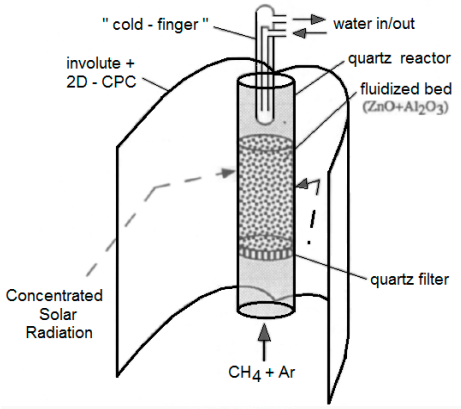	1995 [87]
Diameter= 45 mm, thickness 2.5 mm	$NiFe_2O_4$ – ZrO_2 /N_2	quartz tube	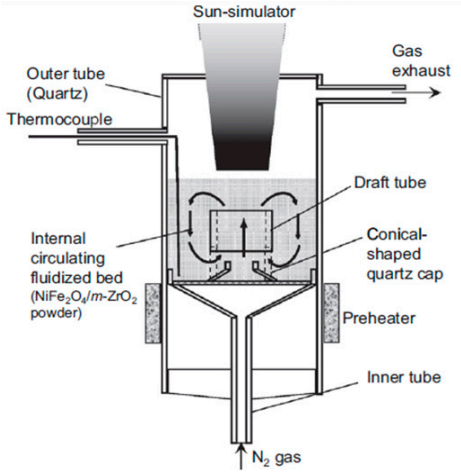	2008 [88]
25mm in diameter, thickness 1.5mm, height 25cm.	CaO or $CaCO_3$ /H_2O,Ar,CO_2	quartz tube	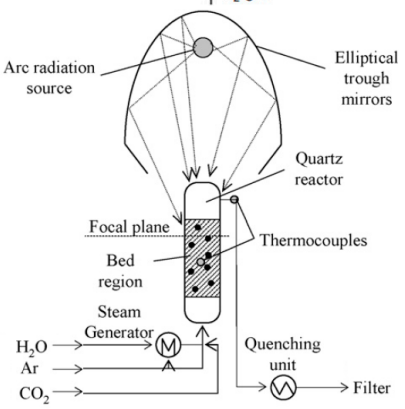	2009 [89]

 doi:10.20944/preprints202407.1069.v1

420mm in length, 62.3mm in inner diameter, and 7mm in thickness	Coke/CO_2	Stainless steel with a quartz window	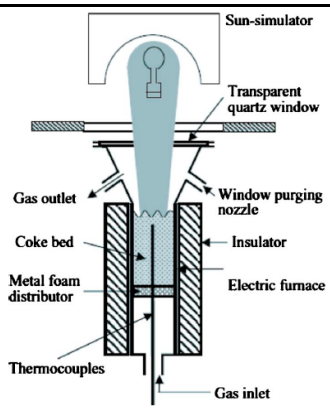	2010 [70]
The inner diameter was 45 mm, and the thickness was 2.5 mm.	$NiFe_2O_4$ /vapor	Stainless steel tube with a quartz cap	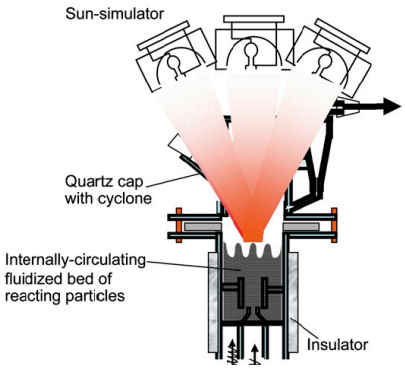	2011 [29]
length 420 mm, inner diameter 62.3 mm, thickness 7 mm	Coke/Ar-vapor CeO_2/N_2	Stainless steel tube (SUS310S) with a quartz window	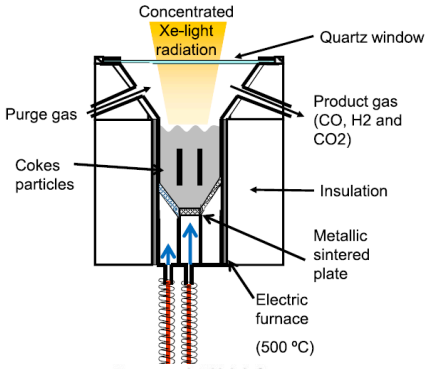	2015 [71,74]
42 cm diameter at the top	quartz sand particles/air	Inconel and stainless steel, with a quartz window	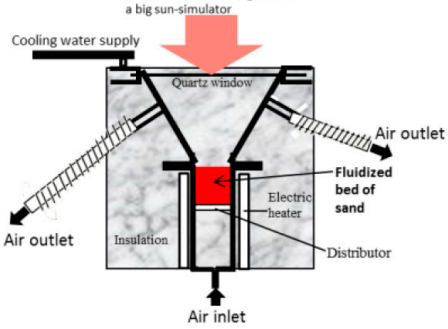	2016 [90]

 doi:10.20944/preprints202407.1069.v1

0.2 m long and 0.3 m internal diameter at the top and 0.007 m thick	quartz particles /N_2	Stainless steel tube with quartz window (5 mm thick)	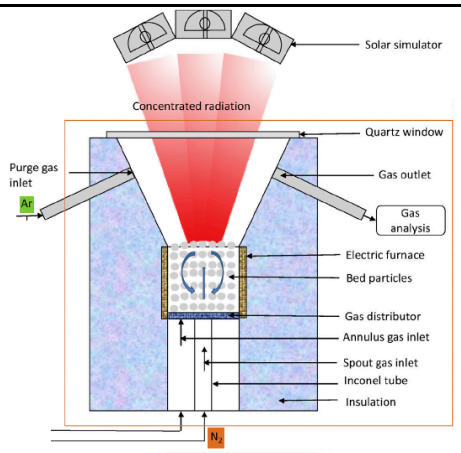	2018 [91]
35.6 cm long and 2.54 cm outer diameter	Iron Aluminate ($FeAl_2O_4$) / N_2	Silicon Carbide Cylindrical Tubes (SiC)	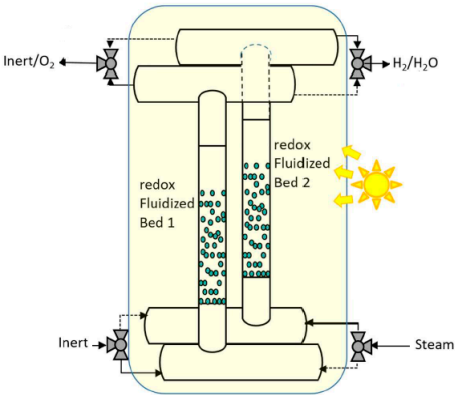	2019 [92]
inside diameter of 7.62 cm and a height of 8 cm	sand, carbo Accucast ID50 y SiC /air	Stainless Steel tube (304)	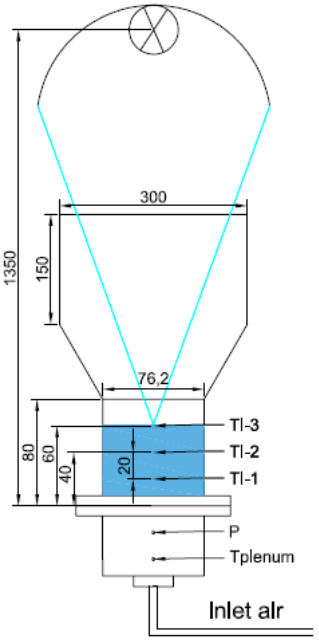	2020 [82]

 doi:10.20944/preprints202407.1069.v1

Tube with 40 mm inner diameter, 10 mm wall thickness, and 1780 mm length	quartz sands/ air	Pure iron metal tube, hot particle container made of stainless steel AISI 304	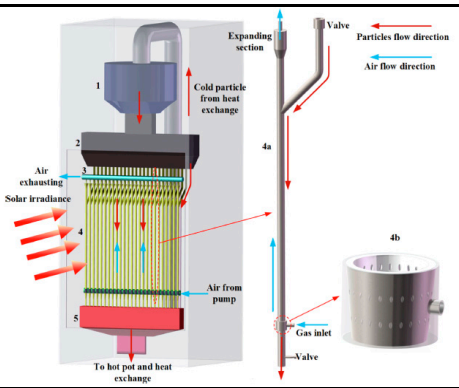	2022 [93]

7. Discussion

Direct Solar Thermal Water-Steam Splitting Using Iron Electrodes at High Temperatures represents a groundbreaking and innovative approach to overcoming some of the most pressing challenges in the renewable energy and hydrogen production sectors, particularly in regions blessed with high solar radiation. This cutting-edge technology harnesses the boundless and eco-friendly power of the sun to produce hydrogen, a versatile and environmentally friendly fuel.

One of the main advantages of this approach lies in the use of a thermochemical iron (Fe) catalyst, which are not only relatively cost-effective but also widely available, mainly in copper slag, is an industrial waste, but it presents a variety of metal oxides that can be used. The search for information on applications of copper slag, no evidence was found of its use as a catalyst material to produce hydrogen, through thermolysis. However, it was determined that the copper slag in Chile has a significant concentration of fayalite, which is composed of two moles of iron oxide (FeO) and one mole of silicon oxide (SiO_2).

This utilization not only reduces the overall cost of the process but also enhances its sustainability and feasibility for large-scale implementation. It's worth noting that the United States Geological Survey (USGS) estimates massive iron ore reserves, further underscoring the accessibility of this material. For instance, in 2017, gross iron ore reserves were estimated at a staggering 170,000 million metric tons, with an iron content of approximately 82,000 million metric tons. However, the 2016 production was a mere 2,106 million metric tons, highlighting the vast untapped potential.

Furthermore, the technology's ability to efficiently split water into hydrogen (H_2) and oxygen (O_2) at high temperatures is of paramount significance. It offers a compelling solution for storing excess solar energy as hydrogen, which can be effectively utilized in fuel cells or other applications during periods of reduced or no sunlight. This effectively addresses one of the most critical issues plaguing solar power – intermittency – and contributes to the creation of a more dependable and consistent energy supply. Nevertheless, it's essential to acknowledge that the high operating temperatures exert considerable stress on the materials, particularly the electrodes and electrolyzer. This necessitates the development of advanced engineering solutions to ensure the technology's longevity, durability, and cost-effectiveness over the long term. Furthermore, optimizing the system design and energy conversion efficiency remains a significant challenge to enhance the competitiveness of this process relative to other hydrogen production methods.

Finally, while this technology boasts immense potential, its practicality and impact are inherently linked to the solar resources and local conditions of the region in which it's deployed. Geographical areas blessed with abundant sunlight stand to reap the greatest benefits, making this innovation an ideal fit for regions with high solar potential. As we continue to refine and develop this technology, it has the potential to play a pivotal role in transitioning towards a more sustainable and environmentally friendly energy landscape.

8. Conclusions

Direct solar thermal water splitting using Fe electrodes at high temperatures is a promising advancement in the field of renewable energy and hydrogen production. By leveraging solar power

 doi:10.20944/preprints202407.1069.v1

and affordable materials, it offers a sustainable and scalable solution to the challenges of clean hydrogen production. As this technology matures and overcomes its current challenges, it has the potential to play a vital role in the transition to a more sustainable and greener energy future, reducing our reliance on fossil fuels and lowering carbon emissions across various industries.

According to data collected from the review of scientific literature, iron will precipitate in the form of ferrous oxide, hematite and magnetite during the oxidation of iron in steam at high temperature, generating hydrogen. Therefore, it is valid to assume that iron, iron oxide or other metal oxides present in slags, such as copper slag, will also precipitate rust and hydrogen. The theoretical thermodynamic and electrochemical aspects of the reaction of metal oxides with water vapor are fundamental for the design of the solar reactor, as well as for an adequate selection of the catalyst metal.

Future recommendations will be aimed at determining whether mineral waste (copper slag) containing metal oxides (iron oxides) are feasible to be used as thermocatalytic materials for the production of hydrogen. For this reason, a morphological and thermochemical characterization of the copper slag produced in Chile will be carried out to determine its subsequent use in a water splitting using a thermochemical solar reactor.

Future research holds significant promise for advancing this technology and addressing various challenges. Here are some key areas of research that can help further develop this innovative approach: (i) Material Science and Corrosion Resistance, (ii) Efficiency Enhancement, (iii) Thermochemical Cycle Optimization, (iv) Integrated Energy Storage, (v) Economic Viability, (vi) Long-term Durability and Reliability, (vii) Scalability and Modular Design, (viii) Hydrogen Purity and Quality and (ix) Market Integration and Policy Support incentives to encourage the adoption of solar thermal water-steam splitting to make this technology more efficient, cost-effective, and environmentally friendly. By addressing these research areas, we can potentially overcome the current challenges and pave the way for its widespread adoption as a clean and sustainable method for hydrogen production.

Author Contributions: Conceptualization, M.F. and F.M.G.M.; methodology, M.F. and F.M.G.M.; validation, A.S., E.F., D.P. A.Sa. and N.T.; investigation, M.F., N.T. D.P. and F.M.G.M.; writing—original draft preparation, M.F. and F.M.G.M.; writing—review and editing, M.F, A.Sa E.F., D.P, A.S., N.T. and F.M.G.M.; visualization M.F., A.S., and F.M.G.M.; supervision, F.M.G.M. All authors have read and agreed to the published version of the manuscript.

Funding: This research received no external funding.

Acknowledgments: The authors would like to thank the Programa de Doctorado en Energía Solar of the Universidad de Antofagasta, Chile. The authors are grateful for the support of ANID-Chile through the research projects FONDECYT Iniciación 11230550 and ANID/ FONDAP 1522A0006 Solar Energy Research Center SERC-Chile.

Conflicts of Interest: The authors declare no conflicts of interest.

References

1. Siegel, N.P.; Miller, J.E.; Ermanoski, I.; Diver, R.B.; Stechel, E.B. Factors Affecting the Efficiency of Solar Driven Metal Oxide Thermochemical Cycles. *Ind Eng Chem Res* 2013, *52*, 3276–3286.
2. Monnerie N. *Green Hydrogen Production at DLR*; 2023;
3. International Energy Agency, I. *Global Hydrogen Review 2022*; 2022;
4. Whitney, W.R. The Corrosion of Iron. *J Am Chem Soc* **1903**, *25*, 394–406, doi:10.1021/ja02006a008.
5. Dunn, J.S. The High Temperature Oxidation of Metals. *Proceedings of the Royal Society of London. Series A, Containing Papers of a Mathematical and Physical Character* **1926**, *111*, 203–209, doi:10.1098/rspa.1926.0062.
6. Tuck, C.W.; Odgers, M.; Sachs, K. *THE OXIDATION OF IRON AT 950°C IN OXYGEN/WATER VAPOUR MIXTURES**; 1969; Vol. 9;.
7. Nakamura, T. Hydrogen Production from Water Utilizing Solar Heat at High Temperatures. *Solar energy* **1977**, *19*, 467–475, doi:10.1016/0038-092X(77)90102-5.
8. Steinfeld, † A; Sanders, S.; Palumbo, R. Design Aspects of Solar Thermochemical Engineering-a Case Study: Two-Step Water-Splitting Cycle Using the Fe3O4 / FeO Redox System. *Solar energy* **1999**, *65*, 43–53, doi:10.1016/S0038-092X(98)00092-9.

9. Lede, J.; Lapicque, F.; Villermaux, J. Production of Hydrogen by Direct Thermal Decomposition of Water. *Int. J. Hydrogen Energy* **1983**, *8*, 675–679, doi:10.1016/0360-3199(83)90175-1.
10. Fernandez Saavedra, R. *Bibliographic Review about Solar Hydrogen Production Through Thermochemical Cycles; Revision Bibliografica Sobre La Produccion de Hidrogeno Solar Mediante Ciclos Termoquimicos.*; 2008;
11. Scheffe, J.R.; Steinfeld, A. Oxygen Exchange Materials for Solar Thermochemical Splitting of H2O and CO2: A Review. *Materials Today* 2014, *17*, 341–348.
12. Perez, N. *Electrochemistry and Corrosion Science*; Springer, 2004;
13. Etievant, C. Solar Energy Materials Solar High-Temperature Direct Water Splitting a Review of Experiments in France. *Solar Energy Materials* **1991**, *24*, 413–440, doi:10.1016/0165-1633(91)90080-5.
14. Meredig, B.; Wolverton, C. First-Principles Thermodynamic Framework for the Evaluation of Thermochemical H2 O - Or CO2 -Splitting Materials. *Phys Rev B Condens Matter Mater Phys* **2009**, *80*, doi:10.1103/PhysRevB.80.245119.
15. Abanades, S. Metal Oxides Applied to Thermochemical Water-Splitting for Hydrogen Production Using Concentrated Solar Energy. *ChemEngineering* 2019, *3*, 63.
16. Kodama, T.; Gokon, N. Thermochemical Cycles for High-Temperature Solar Hydrogen Production. *Chem Rev* 2007, *107*, 4048–4077.
17. Young, J. Effects of Water Vapour on Oxidation. In *Corrosion Series*; 2008; Vol. 1, pp. 455–495.
18. Saunders, S.R.J.; Monteiro, M.; Rizzo, F. The Oxidation Behaviour of Metals and Alloys at High Temperatures in Atmospheres Containing Water Vapour: A Review. *Prog Mater Sci* 2008, *53*, 775–837.
19. Belton, G.R.; Richardson, F.D. A Volatile Iron Hydroxide. *Transactions of the Faraday Society* **1962**, *58*, 1562–1572, doi:10.1039/TF9625801562.
20. Mao, Y.; Gao, Y.; Dong, W.; Wu, H.; Song, Z.; Zhao, X.; Sun, J.; Wang, W. Hydrogen Production via a Two-Step Water Splitting Thermochemical Cycle Based on Metal Oxide – A Review. *Appl Energy* 2020, *267*.
21. Robie, R.A.; Hemingway, B.S. *Thermodynamic Properties of Minerals and Related Substances at 298.15 K and 1 Bar (105 Pascals) Pressure and at Higher Temperatures (No. 2131)*; 1995;
22. Barin, I.; Platzhi, G. *Thermochemical Data of Pure Substances*; 1989; Vol. 304; ISBN 3527287450.
23. Navrotsky, A.; Mazeina, L.; Majzlan, J. Size-Driven Structural and Thermodynamic Complexity in Iron Oxides. *Science (1979)* **2008**, *319*, 1635–1638, doi:10.1126/science.1148614.
24. Svoboda, K.; Slowinski, G.; Rogut, J.; Baxter, D. Thermodynamic Possibilities and Constraints for Pure Hydrogen Production by Iron Based Chemical Looping Process at Lower Temperatures. *Energy Convers Manag* **2007**, *48*, 3063–3073, doi:10.1016/j.enconman.2007.05.019.
25. Birks, N.; Meier, G.H.; Pettit, F.S. High-Temperature Corrosion Resistance. *JOM* **1987**, *39*, 28–31, doi:10.1007/BF03257568.
26. Jeong, M.H.; Lee, D.H.; Bae, J.W. Reduction and Oxidation Kinetics of Different Phases of Iron Oxides. *Int J Hydrogen Energy* **2015**, *40*, 2613–2620, doi:10.1016/j.ijhydene.2014.12.099.
27. Schuetze, M. Fundamentals of High Temperature Corrosion. Materials Science and Technology: A Comprehensive Treatment: Corrosion and Environmental Degradation. **2000**, *I+II*, 67–130, doi:10.1002/9783527619306.ch2.
28. Kodama, T.; Bellan, S.; Gokon, N.; Cho, H.S. Particle Reactors for Solar Thermochemical Processes. *Solar Energy* **2017**, *156*, 113–132, doi:10.1016/j.solener.2017.05.084.
29. Gokon, N.; Mataga, T.; Kondo, N.; Kodama, T. Thermochemical Two-Step Water Splitting by Internally Circulating Fluidized Bed of NiFe2O4 Particles: Successive Reaction of Thermal-Reduction and Water-Decomposition Steps. *Int J Hydrogen Energy* **2011**, *36*, 4757–4767, doi:10.1016/j.ijhydene.2011.01.076.
30. Palumbo, R.; Diver, R.B.; Larson, C.; Coker, E.N.; Miller, J.E.; Guertin, J.; Schoer, J.; Meyer, M.; Siegel, N.P. Solar Thermal Decoupled Water Electrolysis Process I: Proof of Concept. *Chem Eng Sci* **2012**, *84*, 372–380, doi:10.1016/j.ces.2012.08.023.
31. Genescá, J.; Meas, Y.; Rodríguez, F.; Mendoza, J.; Durán, R.; Uruchurtu, J.; González, J.G. *Técnicas Electroquímicas Para El Control y Estudio de La Corrosión*; 2002; Vol. 244;.
32. Bircumshaw, L.L.; Riddiford, A.C. Transport Control in Heterogeneous Reactions. *Quarterly Reviews, Chemical Society* **1952**, *6*, 157–185, doi:10.1039/QR9520600157.
33. Hougen, O.A. Diffusion and Heat Exchange in Chemical Kinetics. *J Am Chem Soc* **1956**, *78*, 885–886.
34. Wen, C.Y. Noncatalytic Heterogeneous Solid-Fluid Reaction Models. *Ind Eng Chem* **1968**, *60*, 34–54.
35. Surman, P.L. THE OXIDATION OF IRON AT CONTROLLED OXYGEN PARTIAL PRESSURES-I. HYDROGEN/WATER VAPOUR. *Corros Sci* **1973**, *13*, 113–124, doi:10.1016/0010-938X(73)90023-1.
36. PARK, H.C.; SAKAI, Y.; KIMURA, S.; TONE, S.; OTAKE, T. A Rate Analysis for Oxidation of Porous Reduced Iron with Water Vapor. *JOURNAL OF CHEMICAL ENGINEERING OF JAPAN* **1984**, *17*, 395–399, doi:10.1252/jcej.17.395.
37. Donovan, R.J.; Berra, Y. External Diffusion Effects on Heterogeneous Reactions. In *In Elements of Chemical Reaction Engineering*; 1999; pp. 686–738.
38. Levenspiel, O. *Ingeniería de Las Reacciones Químicas, 3ª Edición*; Reverté, 2010;

39. Klaewkla, R.; Arend, M.; Hoelderich, W.F. *A Review of Mass Transfer Controlling the Reaction Rate in Heterogeneous Catalytic Systems*; INTECH Open Access Publisher Rijeka, 2011; Vol. 5;.
40. Wen, C.Y.; Wang, S.C. Thermal and Diffusional Effects in Noncatalytic Solid Gas Reactions. *Ind Eng Chem* **1970**, *62*, 30–51.
41. Valipour, M.S.; Saboohi, Y. Modeling of Multiple Noncatalytic Gas-Solid Reactions in a Moving Bed of Porous Pellets Based on Finite Volume Method. *Heat and Mass Transfer/Waerme- und Stoffuebertragung* **2007**, *43*, 881–894, doi:10.1007/s00231-006-0154-2.
42. Yuan, J.; Wang, W.; Zhu, S.; Wang, F. Comparison between the Oxidation of Iron in Oxygen and in Steam at 650-750°C. *Corros Sci* **2013**, *75*, 309–317, doi:10.1016/j.corsci.2013.06.014.
43. Young, D.J.; Watson, S. High-Temperature Corrosion in Mixed Gas Environments. *Oxidation of Metals* **1995**, *44*, doi:10.1007/BF01046729.
44. Go, K.S.; Son, S.R.; Kim, S.D. Reaction Kinetics of Reduction and Oxidation of Metal Oxides for Hydrogen Production. *Int J Hydrogen Energy* **2008**, *33*, 5986–5995, doi:10.1016/j.ijhydene.2008.05.039.
45. Li, P.; Guo, H.; Gao, J.; Min, J.; Yan, B.; Chen, D.; Seetharaman, S. Novel Concept of Steam Modification towards Energy and Iron Recovery from Steel Slag: Oxidation Mechanism and Process Evaluation. *J Clean Prod* **2020**, *254*, doi:10.1016/j.jclepro.2019.119952.
46. Fujji, C.T.; Meussner, R.A. The Mechanism of the High-Temperature Oxidation of Iron-Chromium Alloys in Water Vapor. *J Electrochem Soc* **1964**, *111*, 1215, doi:10.1149/1.2425963.
47. Bauer, S.H.; Schott, G.L.; Duff, R.E. Kinetic Studies of Hydroxyl Radicals in Shock Waves. I. The Decomposition of Water between 2400° and 3200°K. *J Chem Phys* **1958**, *28*, 1089–1096, doi:10.1063/1.1744349.
48. Srinivasan, N.K.; Michael, J. V. The Thermal Decomposition of Water. *Int J Chem Kinet* **2006**, *38*, 211–219, doi:10.1002/kin.20172.
49. Homer, J.B.; Hurle, I.R. The Dissociation of Water Vapour behind Shock Waves. *Proceedings of the Royal Society of London. A. Mathematical and Physical Sciences* **1970**, *314*, 585–598, doi:10.1098/rspa.1970.0024.
50. Brockris, J.O.; Reddy, A.K.N. *Electroquimica Moderna Vol.2*; Reverté, 2003;
51. Rahmel, A.; Tobolsk, J. EINFLUSS VON WASSERDAMPF UND KOHLENDIOXYD AUF DIE OXYDATION VON EISEN IN SAUERSTOFF BEI HOHEN TEMPERATUREN*. *Corros Sci* **1965**, *5*, 333, doi:10.1016/S0010-938X(65)90500-7.
52. Khanna, A.S. *Introduction to High Temperature Oxidation and Corrosion*; ASM international, 2002; ISBN 0871707624.
53. Birks, N.; Meier, G.H.; Pettit, F.S. *Introduction to the High Temperature Oxidation of Metals*; Cambridge university press, 2006; ISBN 1139449095.
54. Sanchez-Caldera, L.E.; Griffith, P.; Asm, F.; Rabinowicz, E.E.; Asme, F. *The Mechanism of Corrosion-Erosion in Steam Extraction Lines of Power Stations*; 1988;
55. Lawless, K.R. *The Oxidation of Metals*; 1974; Vol. 37;.
56. Stehle, R.C.; Bobek, M.M.; Hooper, R.; Hahn, D.W. Oxidation Reaction Kinetics for the Steam-Iron Process in Support of Hydrogen Production. *Int J Hydrogen Energy* **2011**, *36*, 15125–15135, doi:10.1016/j.ijhydene.2011.08.074.
57. Stehle, R.C.; Bobek, M.M.; Hahn, D.W. Iron Oxidation Kinetics for H2 and CO Production via Chemical Looping. *Int J Hydrogen Energy* **2015**, *40*, 1675–1689, doi:10.1016/j.ijhydene.2014.11.035.
58. Ávila, J.; Genescá, J. *Más Allá de La Herrumbre 1*; Fondo de cultura económica, 2013; ISBN 6071603196.
59. Kosaka, F.; Hatano, H.; Oshima, Y.; Otomo, J. Iron Oxide Redox Reaction with Oxide Ion Conducting Supports for Hydrogen Production and Storage Systems. *Chem Eng Sci* **2015**, *123*, 380–387, doi:10.1016/j.ces.2014.11.012.
60. McCafferty, E. Thermodynamics of Corrosion: Pourbaix Diagrams. In *Introduction to Corrosion Science*; Springer New York, 2010; pp. 95–117.
61. Pignocco, A.J.; Pellissier, G.E. LEED STUDIES OF OXYGEN ADSORPTION AND OXIDE FORMATION ON AN (011) IRON SURFACE. *Surf Sci* **1967**, *7*, 261–278, doi:10.1016/0039-6028(67)90020-9.
62. Kogan, A. DIRECT SOLAR THERMAL SPLITTING OF WATER AND ON-SITE SEPARATION OF THE PRODUCTS-II. EXPERIMENTAL FEASIBILITY STUDY. *ht. J. Hydrogen Energy* **1998**, *23*, 9–98, doi:10.1016/S0360-3199(97)00038-4.
63. Kodama, T. High-Temperature Solar Chemistry for Converting Solar Heat to Chemical Fuels. *Prog Energy Combust Sci* 2003, *29*, 567–597.
64. Ehlers, J.; Young, D.J.; Smaardijk, E.J.; Tyagi, A.K.; Penkalla, H.J.; Singheiser, L.; Quadakkers, W.J. Enhanced Oxidation of the 9%Cr Steel P91 in Water Vapour Containing Environments. *Corros Sci* **2006**, *48*, 3428–3454, doi:10.1016/j.corsci.2006.02.002.
65. Ketteler, G.; Weiss, W.; Ranke, W.; Schlögl, R. Bulk and Surface Phases of Iron Oxides in an Oxygen and Water Atmosphere at Low Pressure. *Physical Chemistry Chemical Physics* **2001**, *3*, 1114–1122, doi:10.1039/b009288f.
66. Kritzer, P. Corrosion in High-Temperature and Supercritical Water and Aqueous Solutions: A Review. *Journal of Supercritical Fluids* **2004**, *29*, 1–29, doi:10.1016/S0896-8446(03)00031-7.

67. Siegel, N.P.; Ermanoski, I. *A Beam-down Central Receiver for Solar Thermochemical Hydrogen Production*; 2013;
68. Miyaoka, H. Thermochemical Water Splitting by Concentrated Solar Power. In *Lecture Notes in Energy*; Springer Verlag, 2016; Vol. 32, pp. 137–151.
69. Kodama, T.; Gokon, N.; Matsubara, K.; Yoshida, K.; Koikari, S.; Nagase, Y.; Nakamura, K. Flux Measurement of a New Beam-down Solar Concentrating System in Miyazaki for Demonstration of Thermochemical Water Splitting Reactors. In Proceedings of the Energy Procedia; Elsevier Ltd, 2014; Vol. 49, pp. 1990–1998.
70. Kodama, T.; Gokon, N.; Enomoto, S.I.; Itoh, S.; Hatamachi, T. Coal Coke Gasification in a Windowed Solar Chemical Reactor for Beam-down Optics. *Journal of Solar Energy Engineering, Transactions of the ASME* **2010**, *132*, doi:10.1115/1.4002081.
71. Gokon, N.; Izawa, T.; Kodama, T. Steam Gasification of Coal Cokes by Internally Circulating Fluidized-Bed Reactor by Concentrated Xe-Light Radiation for Solar Syngas Production. *Energy* **2015**, *79*, 264–272, doi:10.1016/j.energy.2014.11.012.
72. Bellan, S.; Gokon, N.; Matsubara, K.; Cho, H.S.; Kodama, T. Heat Transfer Analysis of 5kWth Circulating Fluidized Bed Reactor for Solar Gasification Using Concentrated Xe Light Radiation. *Energy* **2018**, *160*, 245–256, doi:10.1016/j.energy.2018.06.212.
73. Koepf, E.; Advani, S.G.; Steinfeld, A.; Prasad, A.K. A Novel Beam-down, Gravity-Fed, Solar Thermochemical Receiver/Reactor for Direct Solid Particle Decomposition: Design, Modeling, and Experimentation. *Int J Hydrogen Energy* **2012**, *37*, 16871–16887, doi:10.1016/j.ijhydene.2012.08.086.
74. Kodama, T.; Gokon, N.; Cho, H.S.; Bellan, S.; Matsubara, K.; Inoue, K. Particle Fluidized Bed Receiver/Reactor with a Beam-down Solar Concentrating Optics: Performance Test of Two-Step Water Splitting with Ceria Particles Using 30-KWth Sun-Simulator. In Proceedings of the AIP Conference Proceedings; American Institute of Physics Inc., November 8 2018; Vol. 2033.
75. Bellan, S.; Kodama, T.; Seok Cho, H.; Kim, J.S. Hydrogen Production by Solar Fluidized Bed Reactor Using Ceria: Euler-Lagrange Modelling of Gas-Solid Flow to Optimize the Internally Circulating Fluidized Bed. *Journal of Thermal Science and Technology* **2022**, *17*, doi:10.1299/jtst.22-00076.
76. Gokon, N.; Hasegawa, T.; Takahashi, S.; Kodama, T. Thermochemical Two-Step Water-Splitting for Hydrogen Production Using Fe-YSZ Particles and a Ceramic Foam Device. *Energy* **2008**, *33*, 1407–1416, doi:10.1016/j.energy.2008.04.011.
77. Kodama, T.; Gokon, N.; Cho, H.S.; Matsubara, K.; Kaneko, H.; Senuma, K.; Itoh, S.; Yokota, S.N. Particles Fluidized Bed Receiver/Reactor Tests with Quartz Sand Particles Using a 100-KWth Beam-down Solar Concentrating System at Miyazaki. In Proceedings of the AIP Conference Proceedings; American Institute of Physics Inc., June 27 2017; Vol. 1850.
78. Gokon, N.; Kumaki, S.; Miyaguchi, Y.; Bellan, S.; Kodama, T.; Cho, H. Development of a 5kWth Internally Circulating Fluidized Bed Reactor Containing Quartz Sand for Continuously-Fed Coal-Coke Gasification and a Beam-down Solar Concentrating System. *Energy* **2019**, *166*, 1–16, doi:10.1016/j.energy.2018.10.036.
79. Kiwan, S.; Soud, Q.R. Numerical Investigation of Sand-Basalt Heat Storage System for Beam-down Solar Concentrators. *Case Studies in Thermal Engineering* **2019**, *13*, doi:10.1016/j.csite.2018.100372.
80. Yang, S.; Wang, J.; Lund, P.D.; Jiang, C.; Li, X. High Performance Integrated Receiver-Storage System for Concentrating Solar Power Beam-down System. *Solar Energy* **2019**, *187*, 85–94, doi:10.1016/j.solener.2019.05.041.
81. Yang, S.; Wang, J.; Lund, P.D.; Jiang, C.; Li, X. Modelling and Performance Evaluation of an Integrated Receiver-Storage for Concentrating Solar Power Beam-down System under Heterogeneous Radiative Conditions. *Solar Energy* **2019**, *188*, 1264–1273, doi:10.1016/j.solener.2019.07.031.
82. Díaz-Heras, M.; Barreneche, C.; Belmonte, J.F.; Calderón, A.; Fernández, A.I.; Almendros-Ibáñez, J.A. Experimental Study of Different Materials in Fluidized Beds with a Beam-down Solar Reflector for CSP Applications. *Solar Energy* **2020**, *211*, 683–699, doi:10.1016/j.solener.2020.07.011.
83. Fresno, F.; Yoshida, T.; Gokon, N.; Fernández-Saavedra, R.; Kodama, T. Comparative Study of the Activity of Nickel Ferrites for Solar Hydrogen Production by Two-Step Thermochemical Cycles. *Int J Hydrogen Energy* **2010**, *35*, 8503–8510, doi:10.1016/j.ijhydene.2010.05.032.
84. Taylor, R.W.; Berjoan, R.; Coutures, P. *SOLAR GASIFICATION OF CARBONACEOUS MATERIALS*; 1983; Vol. 30;.
85. Flamant, G.; Olalde, G. *HIGH TEMPERATURE SOLAR GAS HEATING COMPARISON BETWEEN PACKED AND FLUIDIZED BED RECEIVERS-I*; 1983; Vol. 31;.
86. Flamant, G.; Gauthier, D.; Boudhari, C.; Flitris, Y. *A 50 KW Fluidized Bed High Temperature Solar Receiver: Heat Transfer Analysis*; 1988;
87. Steinfeld, A.; Frei, A.; Kuhn, P.; Wuillemin, D. SOLAR THERMAL PRODUCTION OF ZINC AND SYNGAS VIA COMBINED ZnO-REDUCTION AND CH,-REFORMING PROCESSES. *J Hydrogen Energy* **1995**, *20*, 793–804, doi:10.1016/0360-3199(95)00016-7.

 doi:10.20944/preprints202407.1069.v1

88. Gokon, N.; Takahashi, S.; Yamamoto, H.; Kodama, T. Thermochemical Two-Step Water-Splitting Reactor with Internally Circulating Fluidized Bed for Thermal Reduction of Ferrite Particles. *Int J Hydrogen Energy* **2008**, *33*, 2189–2199, doi:10.1016/j.ijhydene.2008.02.044.
89. Nikulshina, V.; Gebald, C.; Steinfeld, A. CO2 Capture from Atmospheric Air via Consecutive CaO-Carbonation and CaCO3-Calcination Cycles in a Fluidized-Bed Solar Reactor. *Chemical Engineering Journal* **2009**, *146*, 244–248, doi:10.1016/j.cej.2008.06.005.
90. Kodama, T.; Gokon, N.; Cho, H.S.; Matsubara, K.; Etori, T.; Takeuchi, A.; Yokota, S.N.; Ito, S. Particles Fluidized Bed Receiver/Reactor with a Beam-down Solar Concentrating Optics: 30-KWth Performance Test Using a Big Sun-Simulator. In Proceedings of the AIP Conference Proceedings; American Institute of Physics Inc., May 31 2016; Vol. 1734.
91. Bellan, S.; Gokon, N.; Matsubara, K.; Cho, H.S.; Kodama, T. Numerical and Experimental Study on Granular Flow and Heat Transfer Characteristics of Directly-Irradiated Fluidized Bed Reactor for Solar Gasification. *Int J Hydrogen Energy* **2018**, *43*, 16443–16457, doi:10.1016/j.ijhydene.2018.06.033.
92. Hoskins, A.L.; Millican, S.L.; Czernik, C.E.; Alshankiti, I.; Netter, J.C.; Wendelin, T.J.; Musgrave, C.B.; Weimer, A.W. Continuous On-Sun Solar Thermochemical Hydrogen Production via an Isothermal Redox Cycle. *Appl Energy* **2019**, *249*, 368–376, doi:10.1016/j.apenergy.2019.04.169.
93. Jiang, K.; Kong, Y.; Xu, C.; Ge, Z.; Du, X. Experimental Performance of Gas-Solid Countercurrent Fluidized Bed Particle Solar Receiver with High-Density Suspension. *Appl Therm Eng* **2022**, *213*, doi:10.1016/j.applthermaleng.2022.118661.